Pancreatic β-Cell–Specific Deletion of VPS41 Causes Diabetes Due to Defects in Insulin Secretion

Christian H. Burns,[1] Belinda Yau,[2] Anjelica Rodriguez,[1] Jenna Triplett,[1] Drew Maslar,[1] You Sun An,[2] Reini E.N. van der Welle,[3] Ross G. Kossina,[4] Max R. Fisher,[4] Gregory W. Strout,[4] Peter O. Bayguinov,[4] Tineke Veenendaal,[3] David Chitayat,[5,6] James A.J. Fitzpatrick,[4,7,8] Judith Klumperman,[3] Melkam A. Kebede,[2] and Cedric S. Asensio[1]

Diabetes 2021;70:436–448 | https://doi.org/10.2337/db20-0454

Insulin secretory granules (SGs) mediate the regulated secretion of insulin, which is essential for glucose homeostasis. The basic machinery responsible for this regulated exocytosis consists of specific proteins present both at the plasma membrane and on insulin SGs. The protein composition of insulin SGs thus dictates their release properties, yet the mechanisms controlling insulin SG formation, which determine this molecular composition, remain poorly understood. VPS41, a component of the endolysosomal tethering homotypic fusion and vacuole protein sorting (HOPS) complex, was recently identified as a cytosolic factor involved in the formation of neuroendocrine and neuronal granules. We now find that VPS41 is required for insulin SG biogenesis and regulated insulin secretion. Loss of VPS41 in pancreatic β-cells leads to a reduction in insulin SG number, changes in their transmembrane protein composition, and defects in granule-regulated exocytosis. Exploring a human point mutation, identified in patients with neurological but no endocrine defects, we show that the effect on SG formation is independent of HOPS complex formation. Finally, we report that mice with a deletion of VPS41 specifically in β-cells develop diabetes due to severe depletion of insulin SG content and a defect in insulin secretion. In sum, our data demonstrate that VPS41 contributes to glucose homeostasis and metabolism.

Proper temporal release of peptide hormones plays a critical role in the body's ability to maintain homeostasis. Pancreatic β-cells produce insulin and store it within intracellular vesicles, known as insulin secretory granules (SGs), which undergo exocytosis in response to extracellular stimuli (e.g., hyperglycemia). The basic machinery responsible for this regulated exocytosis consists of proteins present both at the plasma membrane and on insulin SGs. Thus, the protein composition of insulin SGs partly dictates their release properties. SGs form at the *trans*-Golgi network (TGN), where they bud as immature granules. These vesicles then undergo a series of maturation steps, which include luminal acidification, processing of proinsulin to insulin, insulin crystallization with zinc, and removal of immature granule markers (1–8). Surprisingly, the exact mechanisms dictating SG biogenesis and maturation, which is thought to determine their molecular composition, remain poorly understood.

VPS41 and VPS39 associate with the VPS class C core proteins to form the homotypic fusion and vacuole protein sorting (HOPS) complex, which acts as a tether for late endosome–lysosome fusion (9–12). Disruption in HOPS impairs delivery of endocytic cargo to lysosome (13) and causes defects in autophagosome clearance (14,15). Independently of its role in HOPS, VPS41 functions in the

[1]Department of Biological Sciences, University of Denver, Denver, CO
[2]Discipline of Physiology, School of Medical Sciences, Charles Perkins Centre, The University of Sydney, Camperdown, New South Wales, Australia
[3]Section of Cell Biology, Center for Molecular Medicine, University Medical Center Utrecht, Utrecht University, Utrecht, the Netherlands
[4]Washington University Center for Cellular Imaging, Washington University School of Medicine, St. Louis, MO
[5]Division of Clinical and Metabolic Genetics, Department of Pediatrics, The Hospital for Sick Children, University of Toronto, Toronto, Ontario, Canada
[6]Prenatal Diagnosis and Medical Genetics Program, Department of Obstetrics and Gynaecology, University of Toronto, Toronto, Ontario, Canada
[7]Departments of Neuroscience and Cell Biology and Physiology, Washington University School of Medicine, St. Louis, MO
[8]Department of Biomedical Engineering, Washington University in St. Louis, St. Louis, MO

Corresponding author: Cedric S. Asensio, cedric.asensio@du.edu

Received 1 May 2020 and accepted 3 November 2020

This article contains supplementary material online at https://doi.org/10.2337/figshare.13184927.

fusion of TGN-derived LAMP carriers with late endosomes (16). Interestingly, gene expression analysis revealed a significant reduction in VPS41 mRNA levels in islets of mice susceptible to develop diabetes (17), and VPS41 variants have been associated with type 2 diabetes in humans, suggesting that they might be a factor contributing to the development of the disease (18). Furthermore, we previously found that VPS41 affects regulated secretion of neuropeptides from neuroendocrine cells and neurons (19). Altogether, this led us to investigate if VPS41 contributes to glucose homeostasis by influencing insulin SG biology.

Using clustered regularly interspaced short palindromic repeats (CRISPR)/Cas9 in rat insulinoma INS-1 cells, we now show that VPS41 is required for proper insulin storage and regulated secretion. Lack of VPS41 decreases SG number and affects their ability to undergo regulated exocytosis, which is concomitant with a defect in sorting of SG transmembrane proteins. We show that a patient mutation of VPS41, which is deficient for HOPS function (20), rescues insulin-regulated secretion in VPS41 knockout (KO) INS-1 cells, indicating VPS41 function in insulin-regulated secretion is independent of HOPS. Finally, we report that mice with a targeted deletion of VPS41 in β-cells develop diabetes due to a defect in insulin SG biogenesis and secretion. These studies, for the first time, implicate VPS41 in regulating β-cell function and control of glucose homeostasis.

RESEARCH DESIGN AND METHODS

Molecular Biology and Plasmids

The human codon-optimized Cas9 and chimeric guide RNA (gRNA) expression plasmid (pX459v2) developed by the Zhang laboratory were obtained from Addgene (21). To generate gRNA plasmids, a pair of annealed oligos (20 base pairs) were ligated into the single gRNA scaffold of pX459v2. The following gRNA sequences were used: forward (rat), 5′-CACCGACTCTCAGACTGAGCTATGG-3′, and reverse (rat), 5′-AAACCCATAGCTCAGTCTGAGAGTC-3′, to generate the INS1 VPS41 KO line. Rat VPS41 lentiviral plasmid was generated by amplifying VPS41 from rat cDNA using the following primers: wild-type (WT) forward, 5′-CCTCCATAGA AGACACCGACTCTAGACACCATGGCGGAAGCAGAGGAG-3′, and WT reverse, 5′-TATGGGTAACCCCCAGATCCACCGGT CTTCTTCATCTCCAGGATGGCA-3′. The PCR products were then subcloned by Gibson ligation into pLenti-cytomegalovirus (CMV)-green fluorescent protein (GFP)-puromycin (Puro). pLenti-CMV-GFP-Puro (22) was a gift from Paul Odgren (plasmid #73582; Addgene). The following primers were used to genotype VPS41 KO INS-1 cells: rVPS41-forward, 5′-ATATGGTACCTGCAGAGAGGACTAAACGAGA-3′, and rVPS41-reverse, 5′-ATATGAGCTCATGGACGTTGCCATC CAAGT-3′. To test for the presence of indels, the resulting PCR products were ligated into pBlueScript II SK. Isolated plasmids from 10 random colonies were then analyzed for the presence of indels by Sanger sequencing. ON-TARGETplus siRNA pools were obtained from Dharmacon (VPS41: 306991) and used as previously described (19). All retention using selective hooks (RUSH) constructs used were generated using pEGFPC3 as a backbone. STR-Linker-KDEL was used as the endoplasmic reticulum (ER) hook. Neuropeptide Y (NPY)-EGFP-streptavidin binding protein (SBP), NPY-pHluorin-SBP, phogrin-GFP-SBP, and VMAT2-GFP-SBP were generated and used as cargo plasmids (23).

Cell Culture and Lentiviral Production

INS-1 cells (derived from male rat; RRID:CVCL_0352; gift from Dr. Peter Arvan, University of Michigan, Ann Arbor, MI) were maintained in RPMI (with 10% FBS, 1 mmol/L Na-pyruvate, and 50 μmol/L β-mercaptoethanol) under 5% CO_2 at 37°C, transfected using Lipofectamine 2000 or FuGENE HD as per the manufacturer's instructions. HEK293T cells were maintained in DMEM (10% FBS) under 5% CO_2 at 37°C. Lentiviruses were produced by transfecting HEK293T cells with pLenti-CMV-Puro, psPAX2, and pVSVG using 1 mg/mL polyethylenimine. CRISPR-Cas9 KO cells were generated by transfection with pX459v2 containing guides with FuGENE HD. Two days posttransfection, cells were treated with 4 μg/mL puromycin for 2 days. KO single clones were expanded prior to sequencing of indels. Cells were routinely tested for the absence of mycoplasma.

Insulin Secretion Assays

Cells plated at 200,000 cells/24 wells were moved to complete media containing 5 mmol/L glucose 18 h prior and to Krebs-Ringer bicarbonate (KRB) buffer supplemented with 1.5 mmol/L glucose 2 h prior and maintained with 5% CO_2 at 37°C. Cells were stimulated in 250 μL KRB supplemented with 40 mmol/L KCl and 16.7 mmol/L glucose or in low-glucose KRB for 2 h. The secreted fraction was spun at 1,000*g* for 5 min to remove debris. Cells were lysed in 500 μL lysis buffer (50 mmol/L Tris-HCl, 300 mmol/L NaCl, 2% v/v Triton X-100, 1 mmol/L phenylmethylsulfonyl fluoride, and 1× protease inhibitor cocktail) on ice for 5 min. Debris was removed by spinning at 21,000*g* for 10 min at 4°C. ELISA was performed as per the manufacturer's instructions (Thermo Fisher Scientific) with secreted fraction diluted 1:2 and cellular fraction diluted 1:10. Blood insulin and islet insulin secretion ELISA was conducted according to the manufacturer's protocol (Crystal Chem Ultra Sensitive Mouse Insulin ELISA kit). For static secretion, islets recovered in medium (RPMI, 10% FBS, and 11.1 mmol/L glucose) for 1 h at 37°C. Ten islets per well (in triplicate) were placed into KRB with no glucose. Islets were transferred to KRB solution containing 2.8 mmol/L glucose, as basal incubation, or 16.7 mmol/L glucose KRB, as stimulatory and incubate at 37°C for 1 h. Islets were subsequently lysed into islet lysis buffer (100 mmol/L Tris, 300 mmol/L NaCl, 10 mmol/L NaF, and 2 mmol/L sodium orthovanadate). Secreted and cellular insulin content was measured via ELISA, while total DNA content was measured by Pico-Green DNA Assay (Quant-iT PicoGreen dsDNA kit; Thermo Fisher Scientific). Proinsulin secretion was monitored by

ELISA (Mercodia). Samples, both cellular and secreted, were diluted 1:2 for the assay. Secretion was normalized to cell content by measuring DNA in the cellular fraction.

Immunoelectron Microscopy

VPS41 KO or hemagglutinin (HA)-VPS41–expressing INS cells were grown in a T25 flask and fixed using freshly made 4% formaldehyde (FA) and 0.4% glutaraldehyde (GA) in 0.1 mol/L phosphate buffer (pH 7.4) by adding an equal amount of fixative to the medium for 5 min. Cells were postfixed using 2% FA and 0.2% GA in 0.1 mol/L phosphate buffer for 2 h and stored in 1% FA at 4°C. Ultrathin cryosectioning and Immunogold labeling were performed as previously described (24). Proinsulin and insulin were detected using mouse anti-proinsulin (GS9A8, 1:10,000; Dr. Ole D. Madsen) and rabbit anti-insulin (25) (provided by Dr. Peter Arvan; 1:10,000) respectively. Primary and bridging (rabbit anti-mouse, 610-4120, 1:250; Rockland Immunochemicals) antibodies were detected by protein A–10-nm gold particles (Cell Microscopy Core, Utrecht, the Netherlands).

Electron Microscopy and Array Tomography

Coverslips were fixed in 2.5% GA and 2% paraformaldehyde (PFA) in 0.15 mol/L cacodylate buffer, pH 7.4, with 2 mmol/L calcium chloride for 5 min at 37°C. Samples were transferred at 4°C, rinsed in 0.15 mol/L cacodylate buffer three times for 10 min each, fixed for 1 h in 1% osmium tetroxide/0.3% potassium ferrocyanide in cacodylate buffer on ice, washed in ultrapure water three times for 10 min each, and stained en bloc for 1 h with 2% aqueous uranyl acetate. Samples were washed in ultrapure water, dehydrated in graded acetone (50%, 70%, 90%, and 100%, two times) for 10 min each, infiltrated with microwave assistance (PELCO BioWave Pro; Ted Pella, Inc., Redding, CA) into LX112 resin, flat-embedded between two slides coated with PTFE release agent (#MS-143XD; Miller-Stephenson Chemical Co., Danbury, CT), and cured at 60°C for 48 h. For transmission electron microscopy (EM) imaging, 70-nm–thin sections were cut using a diamond knife with a 35° angle (DiATOME, Hatfield, PA) and imaged on a JEOL 1400-Plus transmission EM at 120 kV. For tomography, ~90 80-nm sections were taken in serial, placed onto a silicon wafer, and imaged on a field-emission scanning EM (Merlin; Carl Zeiss, Oberkochen, Germany) using the BSD detector. The scanning EM was operated at 8 KeV and a probe current of 0.9 nA. The same 122-μm field of view in each slice was imaged using the Array Tomography routine in ATLAS 5 (Fibics Incorporated, Ottawa, Ontario, Canada) at 10 nm/pixel resolution at 5 ns dwell time with four-line averaging.

Imaging

INS-1 cells were rinsed with PBS, fixed in 4% PFA in PBS, permeabilized in PBS containing 0.1% Triton X-100 for 10 min at room temperature (RT), and blocked in PBS containing 2% BSA, 1% fish skin gelatin, and 0.02% saponin. Primary and secondary antibodies were diluted as reported in Table 1. For exocytosis assays, cells were cotransfected with NPY-pHluorin and NPY-mCherry. One day after transfection, cells were transferred to poly-L-lysine–coated 22-mm glass coverslips. After an additional 2 days, cells were moved to KRB buffer supplemented with 1.5 mmol/L glucose for 2 h and maintained with 5% CO_2 at 37°C. Cells were washed with KRB buffer, coverslips transferred to an open imaging chamber (Life Technologies), and cells imaged focusing on the plasma membrane (determined by the presence of NPY-mCherry–positive docked vesicles) using a spinning disk. Images were collected for 100 ms at 10 Hz at RT with a 63× objective (Oil Plan Apo numerical aperture 1.49) and an ImagEM X2 EM-CCD camera (Hamamatsu, Hamamatsu City, Japan). Following baseline data collection (15 s), an equal volume of two times KRB buffer containing 114 mmol/L KCl (60 mmol/L final) and 32.65 mmol/L glucose (16.7 mmol/L final) was added to stimulate secretion, and cells were imaged for an additional 45 s. Cells were incubated with KRB containing 50 mmol/L NH_4Cl, pH 7.4, to reveal total fluorescence. Videos were exported as TIFs. Events were quantified within 10 s of basal stimulation and 10 s poststimulation (15 s after high K+ addition). Event length was calculated from time event remained at 20% above baseline. For Fura imaging, cells were plated onto poly-L-lysine–coated imaging dishes and allowed to adhere in media for 2 days. Cells were incubated in KRB solution with 500 nmol/L Fura-2 AM (Life Technologies) for 30 min, washed with basal solution, imaged using a CoolSNAP HQ2 camera with 6.21 μm/pixel using a 40× oil objective (1.3

Table 1—Antibodies used in this study

Antibody target	Source	Dilution (application)
VPS41 (mouse)	Santa Cruz Biotechnology (D-12)	1:100 (Western)
Tubulin (mouse)	DSHB (E-7)	1:500 (Western)
Actin (mouse)	DSHB (JLA20)	1:500 (Western)
Synaptophysin (mouse)	Synaptic Systems (MMS-618R)	1:2,000 (Western)
PC1/3 (rabbit)	Richard Mains (gift)	1:500 (Western)
TFE3 (rabbit)	Cell Signaling Technology (14,779)	1:500 (IF)
Insulin (mouse)	Sigma-Aldrich (K36AC10)	1:1,000 (IF)
HA (rat)	Sigma-Aldrich (3F10)	1:1,000 (IF)
Phogrin (rabbit)	Zippy from John Hutton	1:100 (Western)
Proinsulin (mouse)	DSHB (GS-9A8)	1:500 (IF)

DSHB, Developmental Studies Hybridoma Bank; IF, immunofluorescence.

numeral aperture). Images were binned (two by two), and cells were excited by 340 nm and 380 nm light every 500 ms with a 100-ms interval between exposures. Cells were imaged for 45 s under basal conditions prior to perfusing cells with a 90 mmol/L K+ KRB solution for 45 s. RUSH assays have been described before (23).

Density Gradient Fractionation

Equilibrium sedimentation through sucrose was performed as previously described (19). Fractions (750 μL each) collected from the top were analyzed by quantitative fluorescence immunoblotting using a FluorChem imager (ProteinSimple). Insulin concentration in the fractions was determined by ELISA as before, after diluting fraction 1:4 in lysis buffer for 5 min and then diluting sample 1:5 in ELISA diluent.

Epidermal Growth Factor Degradation Assay

INS-1 cells washed twice with PBS were serum-starved for 2 h in DMEM with 0.1% BSA (GoldBio). After two washes with PBS on ice, cells were incubated with epidermal growth factor (EGF)–Alexa Fluor 647 (Thermo Fisher Scientific) at a concentration of 1 μg/mL for 1 h on ice. Unbound EGF was removed by washing with ice-cold PBS in presence of 0.5% BSA. Cells were chased for the indicated times at 37°C before fixation with 4% PFA in PBS for 30 min on ice. Cells were imaged using a spinning-disk confocal microscope.

Mouse Housing and Breeding

Mice were bred at the Lab Animal Services Facility (Bosch Institute, The University of Sydney) and transferred to the Charles Perkins Centre (The University of Sydney) for experimental procedures. All mice were fed a standard laboratory chow (13% calories from fat, 65% carbohydrate, and 22% protein from Gordon's Specialty Stock Feeds; Yanderra, New South Wales, Australia). $VPS41^{fl/fl}$ mice (26) were crossed with $Ins1^{cre}$ mice (strain 026801; The Jackson Laboratory) to generate third-generation $VPS41^{fl/fl}$, $Ins1^{cre/+}$ mice and their littermate controls for experiments. Male and female animals were combined for all of the experiments. Mice were maintained on a 12-h light/dark cycle (0700/1900 h) and given ad libitum access to food and water. Experiments were carried out in accordance with the National Health and Medical Research Council (Australia) guidelines for animal research and approved by The University of Sydney Animal Experimentation Ethics Committees (Camperdown, New South Wales, Australia).

Glucose Tolerance Test

Mice were fasted 5 h and then analyzed prior to intraperitoneal glucose tolerance test by EchoMRI to calculate dose of 2 mg/kg glucose to lean mass. Mice were tail tipped for basal blood glucose and insulin measurement and then injected with a 25% glucose solution in injectable water via intraperitoneal route. Blood was collected at 15 min for fed insulin measurement and at the following time points: 15, 30, 45, 60, 90, and 120 min for glucose measurements.

Fluorescent Immunohistochemistry

Whole pancreas was imbedded with paraffin. Thin sections were deparaffinized and rehydrated for 3 min in the following solutions: two times xylene rinse solution, one time 50% xylene/50% ethanol, one time 100% ethanol, one time 95% ethanol, one time 80% ethanol, one time 75% ethanol, one time 50% ethanol, and one time double-distilled H_2O. Slides were washed two times for 3 min in wash buffer (PBS with 0.1% BSA and 0.01% NaN_3). Nonspecific antibody association was blocked with two drops of blocking solution (Dako). Primary antibody was diluted in dilution buffer (Dako), 100 μL/section, and incubated overnight at 4°C in a humidified chamber. Slices were washed three times with wash buffer for 3 min each. Secondary antibody was diluted in dilution buffer, and 100 μL/slice was added at RT for 1 h. Slices were rinsed with wash buffer two times for 3 min and with PBS two times for 3 min, dried 5 min at RT, and mounted with ProLong Diamond Antifade (Invitrogen).

Statistics

Unless indicated otherwise, statistical analysis was performed using the two-tailed Student *t* test using Excel or Prism.

Data and Resource Availability

No data sets were generated or analyzed during the current study.

RESULTS

Loss of VPS41 Decreases Insulin-Regulated Secretion and Cellular Content in INS-1 Cells

To assess the contribution of VPS41 to insulin secretion, we generated VPS41 KO INS-1 cells using CRISPR/Cas9. The analysis of indels from genomic DNA isolated from these cells revealed the presence of two distinct single-base-pair insertions predicted to mutate the initiator codon for VPS41 (Supplementary Fig. 1*A*). In addition, we could not detect VPS41 protein by Western blot in lysates generated from these cells (Fig. 1*A*). As a control for potential Cas9 off-target effects, we generated a rescue line by stably reintroducing full-length VPS41 with an HA tag (HA-VPS41) using a lentivirus. We confirmed by Western blot that the HA-VPS41 expression level matched endogenous levels and by immunofluorescence against the epitope tag that the rescue construct could be detected in every cell (Fig. 1*A* and Supplementary Fig. 1*B*). As parent INS-1 cells are notoriously heterogeneous, this rescue line represents a good control for our clonal VPS41 KO cells, and we have thus used it for all subsequent experiments.

We next examined insulin secretion and total cellular insulin content from WT, VPS41 KO, and rescue INS-1 cells by ELISA. We observed a reduction in cellular insulin stores as well as in stimulated (17.5 mmol/L glucose and 40 mmol/L KCl) insulin secretion in the KO cell line (Fig. 1*B* and *C*). Importantly, after normalizing secreted values to cellular stores, we still observed a defect in regulated insulin

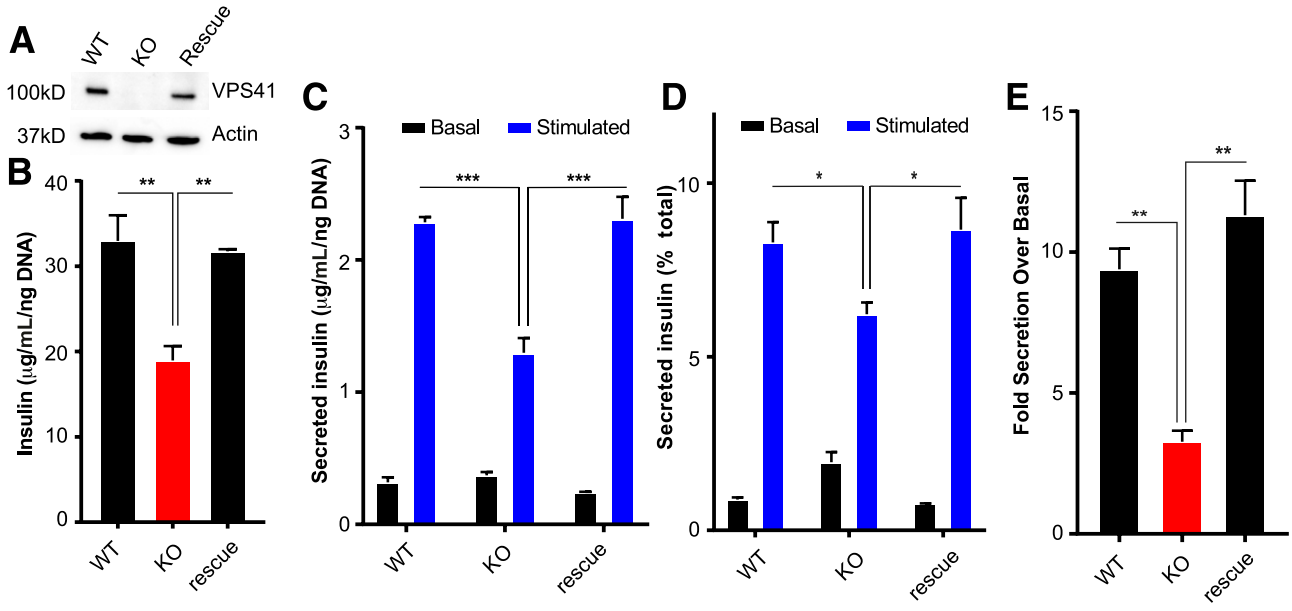

Figure 1—*A*: Representative Western blots showing the levels of VPS41 in WT, VPS41 KO, and HA-VPS41 rescue INS-1 cells. *B*: Total cellular insulin levels under basal conditions determined by ELISA. *C*: Basal and stimulated insulin secretion from KO and rescue INS-1 determined by ELISA. *D*: Insulin secretion relative to cellular insulin stores. *E*: Fold-stimulated insulin secretion over basal insulin secretion. Data indicate mean ± SEM; $n = 3$. $^{*}P < 0.05$, $^{**}P < 0.01$, $^{***}P < 0.001$, secretion data analyzed by one-way ANOVA.

secretion in VPS41 KO cells leading to a decrease in the fold stimulation over basal (Fig. 1*D* and *E*). This indicates that VPS41 not only influences cellular insulin storage, but also partly influences insulin secretion independently of content.

To test whether the decrease in insulin content is caused by a decrease in insulin production, we measured proinsulin levels in cellular lysates by ELISA. We observed no change between WT and VPS41 KO cells, but VPS41 KO cells displayed slightly increased cellular stores of proinsulin compared with rescue cells, indicating no pronounced decrease in synthesis (Supplementary Fig. 2*A*). In addition, VPS41 KO cells showed no difference in proinsulin secretion (Supplementary Fig. 2*B–D*), indicating that proinsulin is not being secreted constitutively. By immunofluorescence, proinsulin distribution remained unchanged among WT, KO, and rescue INS-1 cells (Supplementary Fig. 2*E*). We also determined proinsulin to insulin processing by measuring proinsulin levels at different time points following protein synthesis inhibition with cycloheximide (10 μg/mL). We did not observe any changes in proinsulin levels by Western blot (Supplementary Fig. 2*F*) or immunofluorescence (Supplementary Fig. 2*G*), indicating no significant change in processing. In sum, we conclude that VPS41 plays a role in cellular insulin content and regulated secretion in β-cells. This is consistent with our previous data in neurons and neuroendocrine cells (19).

The Effect of VPS41 on Cellular Insulin Content and Regulated Secretion Is Independent of HOPS

Human patients carrying a point mutation within VPS41 ($VPS41^{S285P}$) exhibit neurological defects without any endocrine dysregulation (20). As this point-mutant results in impaired HOPS function (20), we reasoned that this could be a helpful tool to distinguish between HOPS-dependent and -independent effects of VPS41. Thus, we stably expressed an HA-tagged rat $VPS41^{S284P}$ (S285P equivalent in rat) in VPS41 KO INS-1 cells (Fig. 2*A*). We next examined a HOPS-specific defect in endolysosomal fusion, which results in impaired EGF degradation. Specifically, we incubated cells with fluorescently labeled EGF and looked at the remaining fluorescence after a 90-min chase.

Expression of HA-VPS41 WT in VPS41 KO INS-1 cells rescued the defect in EGF degradation (Fig. 2*B*). In contrast, HA-$VPS41^{S284P}$–expressing cells displayed a defect in EGF degradation similar to VPS41 KO cells, indicating a defect in HOPS (Fig. 2*B*) as observed in other cell types (20). Strikingly, we observed that this mutant rescued insulin secretion and insulin content (Fig. 2*C–F*) phenotypes observed in VPS41 KO INS-1 cells to a similar extent as VPS41-HA WT (rescue) (Fig. 1). This finding indicates that the S284P mutation enables VPS41 to function in the regulated secretory pathway independent of the HOPS complex. Consequently, the role of VPS41 in cellular insulin content and regulated secretion is independent of HOPS functionality.

The Absence of VPS41 Leads to a Decrease in Insulin SG Number

The decrease in insulin cellular content prompted us to determine whether the absence of VPS41 influences the amount of insulin per vesicle (and thus their density)

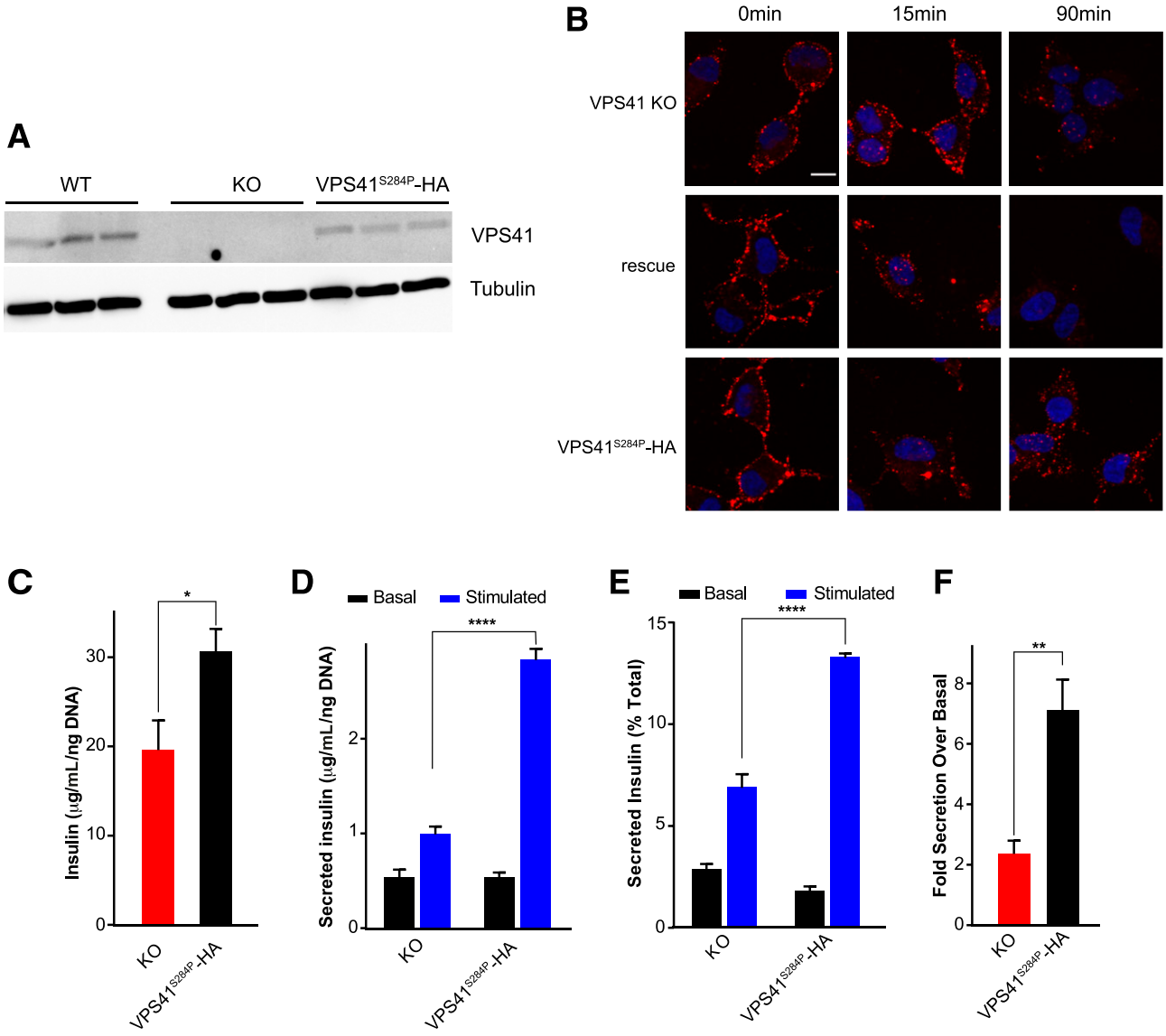

Figure 2—*A*: Representative Western blot showing the levels of VPS41 in WT, VPS41 KO, and HA-VPS41^{S284P} rescue INS-1 cells. *B*: Representative images of indicated cells incubated with EGF–Alexa 647 before or after a short (15-min) or long (90-min) chase. *C*: Total cellular insulin levels of KO and HA-VPS41^{S284P} rescue INS-1 cells under basal conditions determined by ELISA. *D*: Basal and stimulated insulin secretion from KO and HA-VPS41^{S284P} rescue INS-1 cells determined by ELISA. *E*: Insulin secretion relative to cellular insulin stores. *F*: Fold-stimulated insulin secretion over basal insulin secretion. Data indicate mean ± SEM; $n = 3$. *$P < 0.05$, **$P < 0.01$, ****$P < 0.001$, secretion data analyzed by one-way ANOVA. Scale bar, 10 μm.

and/or the number of SGs accumulating intracellularly. For this, we relied first on equilibrium sedimentation through sucrose to separate organelles based on their density and determined insulin distribution within the gradient by ELISA. We observed no change among WT, KO, and rescued cells, suggesting no change in SG density (Fig. 3*A*). Analysis of thin sections by EM (Fig. 3*B* and *C*) or of entire cells by three-dimensional array tomography (Supplementary Videos 1 and 2) revealed a decrease in the number of SGs in VPS41 KO cells. Altogether, these data indicate that the absence of VPS41 decreases the number of SGs, but does not influence insulin packaging.

VPS41 KO Cells Display Normal TGN Budding Kinetics, but Transmembrane Protein Missorting

We next tested whether the decrease in SG number observed in VPS41 KO cells could be a consequence of a budding defect from the TGN. For this, we relied on the RUSH system (27), which allows us to synchronize and visualize the movement of cargoes along the secretory pathway. This assay, which we recently optimized for endocrine cells (23), uses localized expression of streptavidin within the ER as a hook to trap a coexpressed secretory cargo fused to streptavidin-binding peptide. Addition of biotin leads to the release of a discrete, synchronized wave of the secretory cargo; in this case,

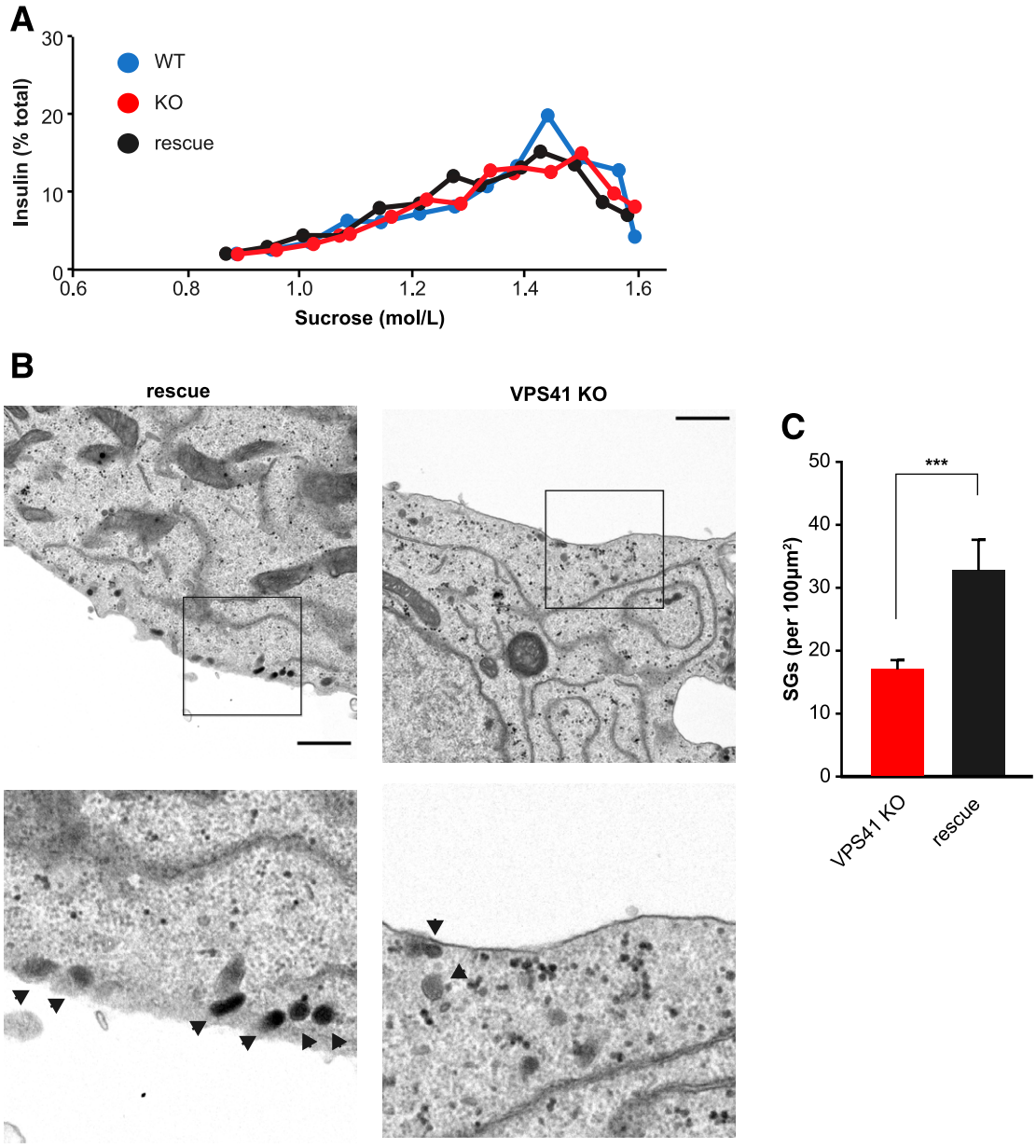

Figure 3—*A*: Postnuclear supernatants obtained from WT, VPS41 KO, and HA-VPS41 rescue INS-1 cells were separated by equilibrium sedimentation through 0.6–1.6 mol/L sucrose. Fractions were collected from the top of the gradient. Insulin levels were determined by ELISA in each fraction. The graph indicates the percentage of total gradient insulin from one experiment. Similar results were obtained in an additional independent experiment. *B*: Representative thin-section EM images of VPS41 KO and rescue INS-1 cells. Arrowheads point at SGs. Scale bars, 1 μm. *C*: Quantification of total SGs per cell normalized to the area of the cell. Data indicate mean ± SEM; $n = 45$ cells for KO and 18 cells for rescue. ***$P < 0.001$.

NPY-GFP-SBP, a soluble marker of SGs. Using live imaging, we monitored the movement of NPY-GFP-SBP along the secretory pathway. Upon addition of biotin, NPY-GFP-SBP trafficked from the ER to the Golgi, followed by its incorporation into post-Golgi carriers in VPS41 KO and rescue cells. By measuring changes in fluorescence, we calculated that the rate of TGN exit remained unchanged between the two cell lines (Fig. 4*A* and Supplementary Videos 3 and 4). Next, we determined whether NPY-GFP-SBP sorted to SGs properly by determining the degree of colocalization 24 h after releasing the cargo from its hook. We found that the wave of NPY-GFP-SBP colocalized with endogenous insulin in both cell lines (Fig. 4*B* and *C*). Furthermore, immuno-EM analysis confirmed that proinsulin and insulin sorted properly to SGs (Supplementary Fig. 3). These data indicate that the budding kinetics and sorting of soluble SG cargoes remain unaffected. We next looked at the behavior of a transmembrane SG marker (phogrin-GFP-SBP) using the RUSH system. Again, we found no difference in TGN exit rates (Fig. 4*D*). However,

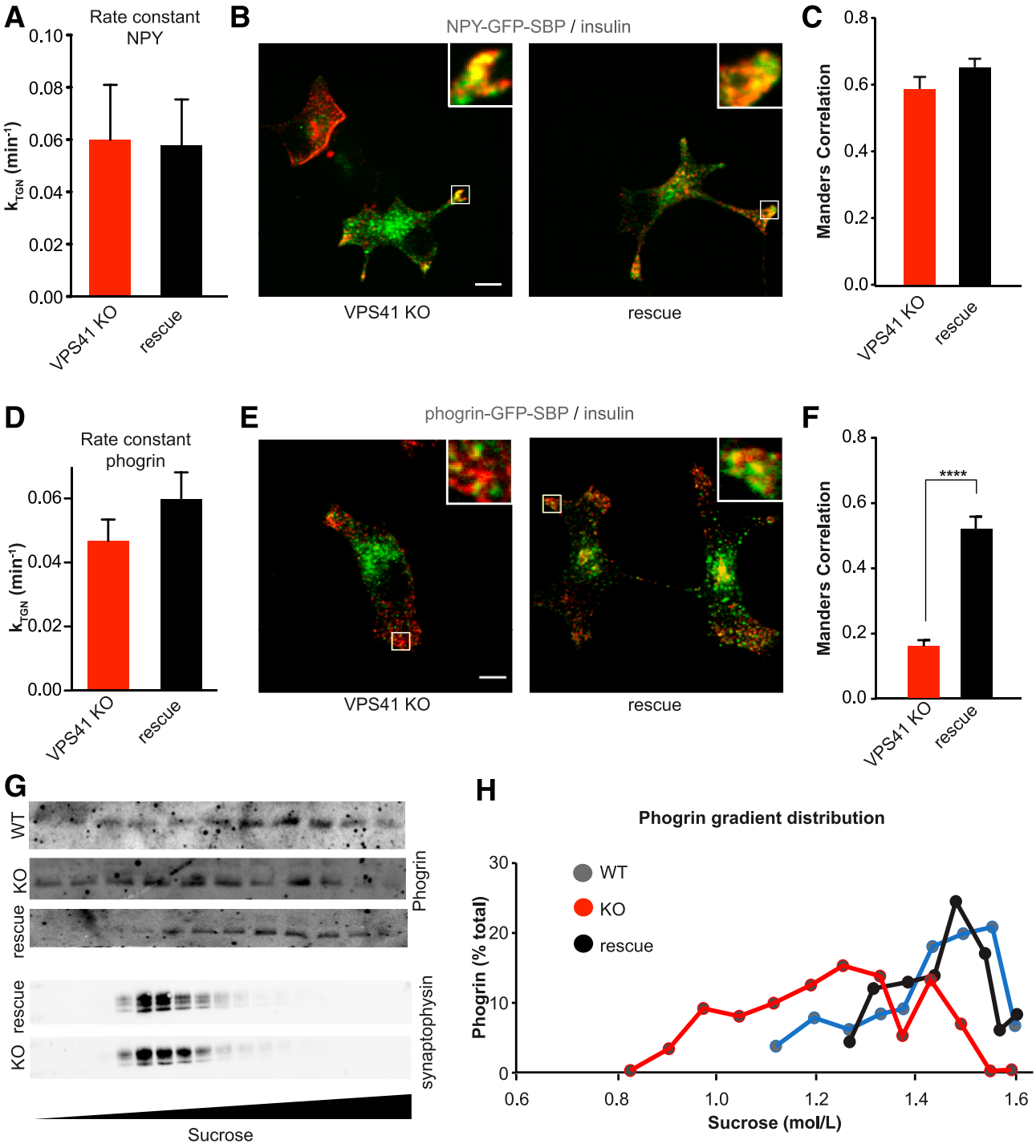

Figure 4—*A*: TGN rate constants of NPY-GFP-SBP from VPS41 KO and HA-VPS41 rescue INS-1 cells after induction of cargo wave via biotin addition. Data indicate mean ± SEM; $n = 9$ cells for rescue and $n = 5$ cells for KO, two independent transfections. *B*: Representative images of NPY-GFP-SBP costained with insulin 24 h post–biotin addition. Scale bar, 10 μm. *C*: Manders colocalization coefficient of NPY-GFP-SBP colocalization with insulin signal in VPS41 KO and rescue. Data indicate mean ± SEM; $n = 24$ cells for rescue and $n = 24$ cells for KO, two independent transfections. *D*: TGN rate constants of phogrin-GFP-SBP from VPS41 KO and HA-VPS41 rescue INS-1 cells after induction of cargo wave via biotin addition. Data indicate mean ± SEM; $n = 7$ cells for rescue and $n = 7$ cells for KO, two independent transfections. *E*: Representative images of phogrin-GFP-SBP costained with insulin 24 h post–biotin addition. Scale bar, 10 μm. *F*: Manders colocalization coefficient of phogrin colocalization with insulin signal in VPS41 KO and rescue. Data indicate mean ± SEM; $n = 21$ cells for rescue and $n = 18$ cells for KO, two independent transfections. ****$P < 0.0001$. *G*: Postnuclear supernatants obtained from WT, VPS41 KO, and HA-VPS41 rescue INS-1 cells were separated by equilibrium sedimentation through 0.6–1.6 mol/L sucrose as described in Fig. 3. Fractions were assayed for phogrin and synaptophysin (p38) by quantitative fluorescence immunoblotting. *H*: The graph quantifies phogrin immunoreactivity in each fraction as a percentage of total gradient immunoreactivity from one experiment. Similar results were obtained in an additional independent experiment.

we observed a striking decrease in phogrin colocalization with endogenous insulin in VPS41 KO cells (Fig. 4*E* and *F*). This suggests that the absence of VPS41 does not affect TGN budding rates per se but influences SG transmembrane protein composition.

To confirm these findings, we relied on an alternative approach and looked at the distribution of endogenous phogrin after equilibrium sedimentation through sucrose. We observed that phogrin was shifted toward lighter fractions in VPS41 KO cells (Fig. 4*G* and *H*). This effect appears to be specific to SGs, as sedimentation of synaptophysin (p38), a marker of synaptic-like microvesicles, remained unaffected (Fig. 4*G*). These results are consistent with our RUSH data and indicate that phogrin is missorted in absence of VPS41. These data are in line with previous results obtained in PC12 cells (19).

VPS41 KO Cells Exhibit Defective Insulin Granule Exocytosis

We hypothesized that the absence of VPS41 could lead to the formation of "malfunctioning" SGs that are unable to undergo exocytosis in response to a stimulus, which might explain the defect in regulated insulin secretion. We next tested whether the absence of VPS41 leads to an impairment in SG exocytosis. We transfected VPS41 KO and rescue cells with NPY-pHluorin and monitored exocytosis in real time using spinning-disk confocal microscopy (Supplementary Videos 5 and 6). Under basal conditions, we observed very few exocytosis events across the two cell lines (<1 event/μm^2/s [$\times 10^{-4}$]). After stimulation, HA-VPS41 rescue cells showed a robust increase in the number of exocytosis events (55 events/μm^2/s [$\times 10^{-4}$]), whereas in the KO cells, only 12 events/μm^2/s ($\times 10^{-4}$) were observed (Fig. 5*A*). Interestingly, we also found that the few exocytosis events observed in the KO cells exhibited very different kinetics. Indeed, in rescue cells, the large majority of events (>80%) lasted <1 s, but in the KO cells, 50% of events lasted for >1 s, sometimes up to 9 s (Fig. 5*B*). Importantly, this exocytosis defect is not caused by an impairment in the excitability of the cells, as calcium imaging experiments revealed that VPS41 KO and rescue cells displayed similar responses following depolarization (Fig. 5*C*).

Mice With β-Cell–Specific Deletion of VPS41 Develop Diabetes due to a Defect in Insulin Secretion and Content

To explore the physiological role and significance of VPS41 to glucose homeostasis, we generated β-cell–specific VPS41 (βVPS41) KO mice by crossing $VPS41^{fl/fl}$ animals with mice expressing *Cre* under the control of the insulin promoter, *Ins1*-Cre mice (28). β-Cell specificity was confirmed using immunoblotting of different tissues and immunofluorescent staining of islets. Comparison of VPS41 protein levels in lysates prepared from isolated islets revealed a ~75% reduction in βVPS41 KO mice in comparison with their control littermates (Fig. 6*A* and *B*). The remaining 25% accounts for VPS41 expression in non–β-cells of the islets. Importantly, VPS41 levels remained unchanged in whole brain, hypothalamus, and liver lysates, indicating that the deletion is specific (Fig. 6*A* and *B*).

Interestingly, βVPS41 KO mice did not show any changes in body weight, fat, or lean mass at 8 (Fig. 6*C*) or 15 (Supplementary Fig. 4*A*) weeks of age, but these animals develop diabetes characterized by fasting hyperglycemia (Fig. 6*D*) and glucose intolerance (Fig. 6*E*) without changes in insulin sensitivity (Supplementary Fig. 4*E*). At 15 weeks, VPS41 KO mice displayed an even more severe phenotype (Supplementary Fig. 4*B–D*).

The diabetes in βVPS41 KO mice is associated with a pronounced reduction in basal and glucose-stimulated

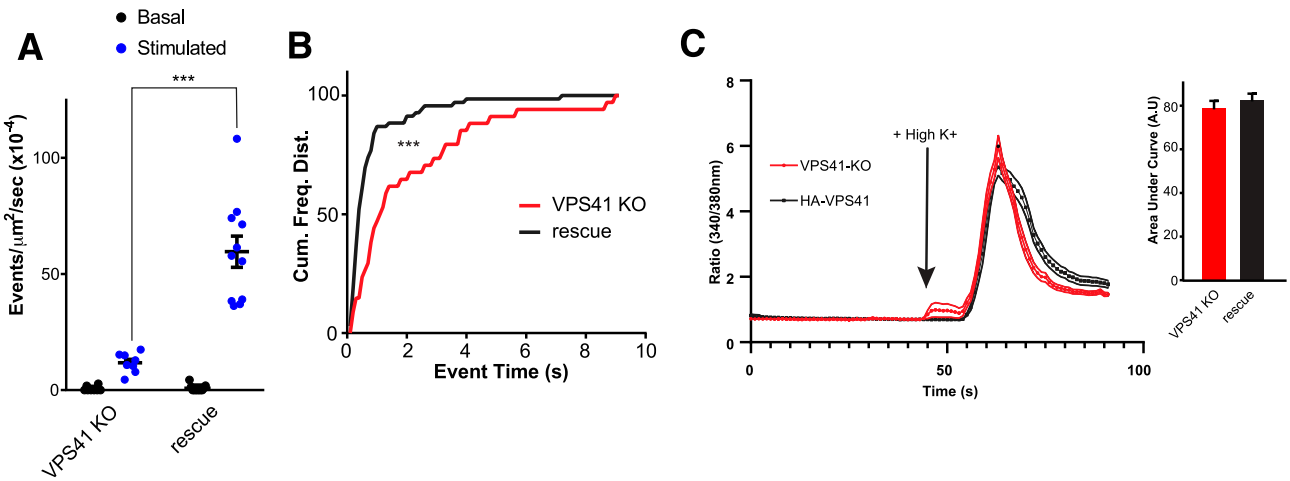

Figure 5—*A*: Quantification of NPY-pHluorin exocytosis events in VPS41 KO and HA-VPS41 rescue INS-1 cells over a 10-s basal or stimulated period. $n = 3$ independent transfections. *B*: Cumulative frequency distribution (Cum. Freq. Dist.) of NPY-pHluorin exocytosis event duration in VPS41 KO and rescue cells ($n = 34$ KO and 69 HA-VPS41 events from three independent transfections). *C*: Average Fura curves in response to depolarization by high K+. Bar graph on the right shows quantification of the area under the curve of calcium imaging (Fura) in response to depolarization (high K^+) in KO and rescue cells ($n = 35$ KO and 38 HA-VPS41 cells). Data indicate mean ± SEM. ***$P < 0.001$. Event number analyzed by one-way ANOVA. Event duration analyzed by Kolmogorov–Smirnov. A.U., arbitrary unit.

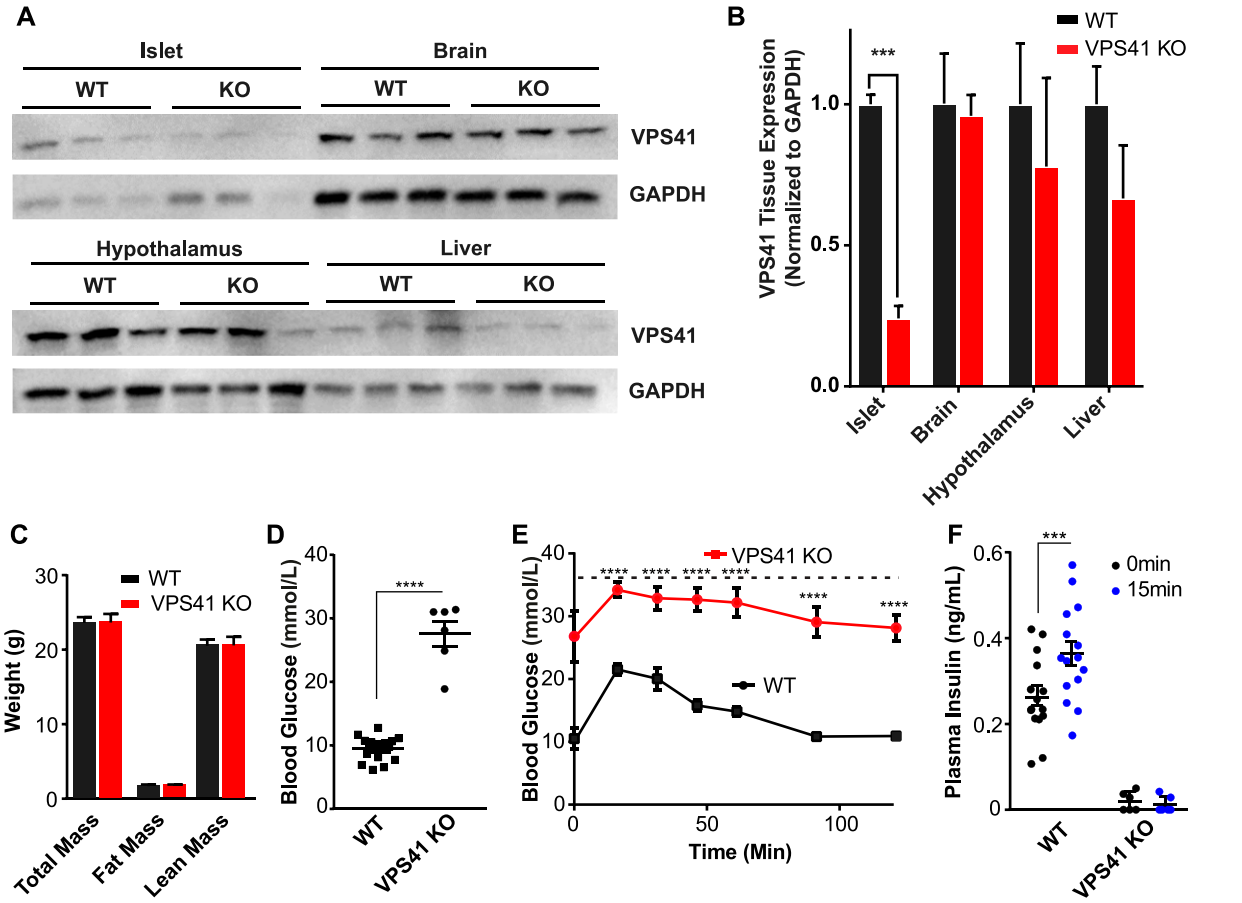

Figure 6—*A*: Representative Western blots of VPS41 protein levels in various tissues from 15-week-old age-matched WT or VPS41 KO mice. *B*: Quantification of VPS41 protein expression levels normalized to GAPDH. Data indicate mean ± SEM; $n = 3$. ***$P < 0.001$. *C*: Fat and lean mass measurements of age-matched 8-week-old WT and VPS41 KO mice. *D*: Blood glucose measurement of mice fasted for 8 h. *E*: Blood glucose measurements during glucose tolerance test. The dashed lines indicate the maximum value of the glucometer. *F*: Circulating blood insulin levels before and 15 min after glucose injection. Data indicate mean ± SEM; KO, $n = 6$; and WT, $n = 15$. ***$P < 0.001$, ****$P < 0.0001$, secretion data analyzed by one-way ANOVA.

insulin levels during the glucose tolerance tests (Fig. 6*F*) and severe depletion of insulin in the islets. Immunofluorescence staining of whole pancreas sections revealed a reduction in insulin levels with different degree of severity between cells, but no apparent change in glucagon (Fig. 7*A*) and no obvious alteration in the proportion of α- and β-cells. In addition, we isolated islets from 15-week-old animals and determined glucose-stimulated insulin secretion in vitro. Consistent with our data in INS-1 cells, we observed a dramatic defect in basal and glucose-stimulated insulin secretion from isolated islets (Fig. 7*B* and *D*), together with a severe reduction in insulin content (Fig. 7*C*). We observed a similar trend for proinsulin (Supplementary Fig. 4*F–I*) in islets isolated from 15-week-old animals. However, glucagon content from isolated islets remained unchanged (Supplementary Fig. 4*J*). Finally, we found a reduction in the number of insulin SGs by EM in islets of VPS41 KO mice (Fig. 7*E* and *F*).

In conclusion, we find that deletion of VPS41 specifically in β-cells leads to an overtly diabetic mouse due to decreased insulin secretion and content. However, this mouse does not exhibit obvious defects in glucagon levels or islet architecture, suggesting again that VPS41 is playing a specific role in the regulation of regulated insulin storage and release, both in vitro and in vivo.

DISCUSSION

Loss of VPS41 from neuroendocrine PC12 cells and neurons leads to defects in peptidergic-regulated secretion (19). SGs can still form in these cells, but they show altered size and morphology. We now show that absence of VPS41 also leads to defects in insulin-regulated secretion and cellular content in β-cells. Thus, although SGs display a wide range of size and cargo content across specialized secretory cells, some of the molecular mechanisms controlling their formation seem conserved between neuroendocrine and endocrine cells and neurons.

We also find that the S285P human mutation, which is unable to rescue HOPS function (20), restores insulin secretion completely, indicating that it is actually possible to isolate HOPS-dependent and -independent functions of VPS41. Furthermore, this observation also helps explain why patients bearing this mutation have no observable

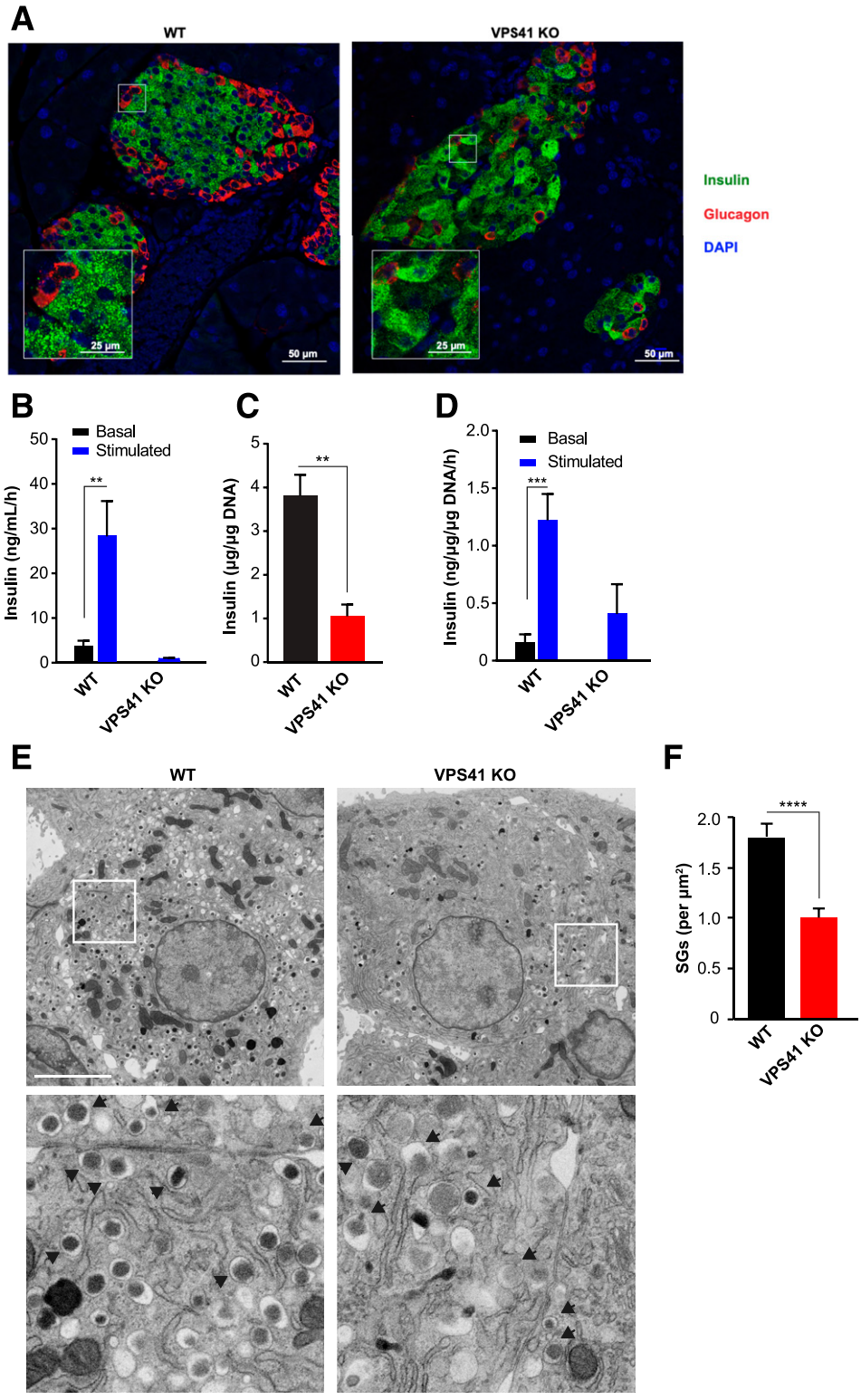

Figure 7—*A*: Representative immunofluorescence images of whole pancreas slices from WT and VPS41 KO mice stained for insulin (green) and glucagon (red). *B*: Stimulated insulin secretion from isolated islets from WT and VPS41 KO mice under basal or high-glucose conditions. *C*: Islet insulin content normalized to DNA content, analyzed by *t* test. *D*: Insulin secretion from isolated islets normalized to islet insulin concentration. Data indicate mean ± SEM; $n = 3$. $^{**}P < 0.01$, $^{***}P < 0.001$, secretion data analyzed by one-way ANOVA. *E*: Representative thin-section EM images of islets from WT and VPS41 KO mice. Arrowheads point at SGs. Scale bar, 5 μm. *F*: Quantification of total SGs per cell normalized to the area of the cell. Data indicate mean ± SEM; $n = 128$ cells for WT from 3 animals and 141 cells from 3 animals. $^{****}P < 0.0001$.

endocrine-associated defects. It might also show that the HOPS-independent function of VPS41 is necessary for survival, since VPS41 KO mice die early during embryogenesis (26). In summary, our data indicate that VPS41 is required for insulin secretion and intracellular storage, and this effect is independent of HOPS.

As the NPY-pHluorin assay did not reveal any changes in the number of basal exocytosis events and as insulin basal secretion remained unchanged in absence of VPS41, it is unlikely that rerouting of soluble-regulated cargoes to the constitutive secretory pathway accounts for the decrease in SGs. We also did not observe a decrease in proinsulin cellular levels, suggesting that insulin production remains unaffected. Finally, the results from the RUSH experiments indicate that the lack of VPS41 does not impair cargo budding. This finding is further substantiated by the lack of excessive accumulation of proinsulin at the Golgi in VPS41 KO cells compared with WT and rescue cells by immunofluorescence. It is thus tempting to speculate that the lack of VPS41 leads to degradation of SGs. Indeed, degradation is an important mechanism by which β-cells maintain insulin granule homeostasis (29,30). Several modes of SG degradation have been described over the years, including macroautophagy, crinophagy, and stress-induced granule degradation, which involve the direct fusion of granules with lysosomes, and Golgi membrane-associated degradation (31–35). As crinophagy and macroautophagy are HOPS-dependent processes (14,36), these pathways probably do not contribute much to granule turnover, as they are likely to be defective in VPS41 KO cells. In the future, it will be interesting to test whether there is an increase in stress-induced granule degradation and/or Golgi membrane-associated degradation in VPS41 KO cells once the molecular mechanisms for these processes are better understood.

In addition, independently from the decrease in cellular insulin content, our results show that the absence of VPS41 leads to a defect in regulated secretion of insulin. Our data suggest that VPS41 might control sorting of transmembrane proteins, which ultimately could influence SG release properties. We have previously proposed that VPS41 functions at the TGN during budding of SGs in neuroendocrine cells (19). Consistent with this, a pool of VPS41 localizes to the TGN (16,19). Alternatively, VPS41 might contribute to SG biogenesis by influencing maturation after budding. Indeed, several cytosolic factors that have recently been implicated in SG biogenesis are typically associated with endocytic and retrograde pathways (37–44). The EARP complex and its interacting partner EIPR-1, for example, contribute to SG cargo sorting (45,46). It is thus tempting to speculate that retrograde pathways might contribute to SG maturation and that VPS41 could influence this process. Interestingly, in addition to a reduction in the number of exocytotic events after stimulation, we observed a change in the release properties of SGs in VPS41 KO cells with an increase in the duration of the events. Thus, we cannot exclude that VPS41 contributes to SG exocytosis directly by interacting with SNAREs or other factors of the exocytosis machinery.

Islets of BTBR mice, which are prone to develop diabetes, exhibit decreased levels of VPS41 gene expression (17). In agreement with this, we now show that mice with a specific deletion of VPS41 in β-cells are overtly diabetic. Indeed, these animals display extreme fasting hyperglycemia and are glucose intolerant due to a defect in insulin content and secretion. Disruption of lysosomal genes such as raptor leads to a very similar phenotype; however, in this case, the defect in secretion seems to be linked to β-cell maturation and early-onset decreases in β-cell mass (47). In contrast, we observed no obvious difference in islet size and morphology in absence of VPS41. Our data indicate that VPS41 plays a significant role in glucose homeostasis and normal physiology. Our findings, together with the identification of several point mutations associated with type 2 diabetes in humans (18), further underline the importance of membrane trafficking in health and disease (48). In particular, our data emphasize the physiological significance of understanding the mechanisms of SG formation at the molecular level. Unraveling the role of cytosolic factors in this process could help reveal potential therapeutic targets for the treatment of metabolic and endocrine-associated diseases.

Acknowledgments. The authors thank Peter Arvan (University of Michigan, Ann Arbor, MI) for the INS-1 cell line and Yoh Wada (Osaka University, Osaka, Japan) for the VPS41$^{fl/fl}$ mice. PC1/3 antibody was a gift from Dick Mains (University of Connecticut, Farmington, CT) and Betty Eipper (University of Connecticut, Farmington, CT).

Funding. The Washington University Center for Cellular Imaging was supported by Washington University School of Medicine, the Children's Discovery Institute of Washington University and St. Louis Children's Hospital (CDI-CORE-2015-505 and CDI-CORE-2019-813 to J.A.J.F.), the Foundation for Barnes-Jewish Hospital (3770 to J.A.J.F.), and the Washington University Diabetes Research Center (P30 DK020579). M.A.K. is supported by a Jennie Mackenzie Philanthropic Fellowship, The University of Sydney. Y.S.A. is a recipient of an Australian Postgraduate Scholarship. J.K. and R.E.N.v.d.W. are supported by the Deutsche Forschungsgemeinschaft FOR2625. This work was supported by American Diabetes Association grant 1-17-JDF-064 and National Institute of General Medical Sciences grants R01 GM124035 and R15 GM116096 to C.S.A.

Duality of Interest. No potential conflicts of interest relevant to this article were reported.

Author Contributions. C.H.B. conducted in vitro experiments, acquired and analyzed data, and wrote the manuscript. B.Y. and Y.S.A. conducted in vivo experiments and acquired and analyzed data. A.R., J.T., D.M., R.E.N.v.d.W., and T.V. conducted in vitro experiments and acquired and analyzed data. R.G.K. and G.W.S. conducted the thin-section EM. M.R.F. and P.O.B. conducted the array tomography experiments. D.C. identified the S285P human mutation. J.A.J.F., J.K., and M.A.K. supervised the study and edited the manuscript. C.S.A. designed the study, analyzed data, supervised the study, and wrote the manuscript. C.S.A. is the guarantor of this work and, as such, had full access to all of the data in the study and takes responsibility for the integrity of the data and the accuracy of the data analysis.

Prior Presentation. A non–peer-reviewed version of this article was submitted to the BioRxiv preprint server (https://www.biorxiv.org/content/10.1101/2019.12.18.867333v1) on 20 December 2019. This work was presented at the 79th Scientific Sessions of the American Diabetes Association, San Francisco, CA, 7–11 June 2019 and at the Keystone Symposium on Diabetes: Glucose Control and Beyond, Santa Fe, NM, 27–31 January 2020.

References

1. Ahras M, Otto GP, Tooze SA. Synaptotagmin IV is necessary for the maturation of secretory granules in PC12 cells. J Cell Biol 2006;173:241–251
2. Borgonovo B, Ouwendijk J, Solimena M. Biogenesis of secretory granules. Curr Opin Cell Biol 2006;18:365–370
3. Dittie AS, Hajibagheri N, Tooze SA. The AP-1 adaptor complex binds to immature secretory granules from PC12 cells, and is regulated by ADP-ribosylation factor. J Cell Biol 1996;132:523–536
4. Hou JC, Min L, Pessin JE. Insulin granule biogenesis, trafficking and exocytosis. Vitam Horm 2009;80:473–506
5. Klumperman J, Kuliawat R, Griffith JM, Geuze HJ, Arvan P. Mannose 6-phosphate receptors are sorted from immature secretory granules via adaptor protein AP-1, clathrin, and syntaxin 6-positive vesicles. J Cell Biol 1998;141:359–371
6. Park JJ, Koshimizu H, Loh YP. Biogenesis and transport of secretory granules to release site in neuroendocrine cells. J Mol Neurosci 2009;37:151–159
7. Takeuchi T, Hosaka M. Sorting mechanism of peptide hormones and biogenesis mechanism of secretory granules by secretogranin III, a cholesterol-binding protein, in endocrine cells. Curr Diabetes Rev 2008;4:31–38
8. Tooze SA. Biogenesis of secretory granules in the trans-Golgi network of neuroendocrine and endocrine cells. Biochim Biophys Acta 1998;1404:231–244
9. Price A, Seals D, Wickner W, Ungermann C. The docking stage of yeast vacuole fusion requires the transfer of proteins from a cis-SNARE complex to a Rab/Ypt protein. J Cell Biol 2000;148:1231–1238
10. Rieder SE, Emr SD. A novel RING finger protein complex essential for a late step in protein transport to the yeast vacuole. Mol Biol Cell 1997;8:2307–2327
11. Seals DF, Eitzen G, Margolis N, Wickner WT, Price A. A Ypt/Rab effector complex containing the Sec1 homolog Vps33p is required for homotypic vacuole fusion. Proc Natl Acad Sci U S A 2000;97:9402–9407
12. van der Beek J, Jonker C, van der Welle R, Liv N, Klumperman J. CORVET, CHEVI and HOPS - multisubunit tethers of the endo-lysosomal system in health and disease. J Cell Sci 2019;132:jcs189134
13. Balderhaar HJ, Ungermann C. CORVET and HOPS tethering complexes - coordinators of endosome and lysosome fusion. J Cell Sci 2013;126:1307–1316
14. Jiang P, Nishimura T, Sakamaki Y, et al. The HOPS complex mediates autophagosome-lysosome fusion through interaction with syntaxin 17. Mol Biol Cell 2014;25:1327–1337
15. Takáts S, Pircs K, Nagy P, et al. Interaction of the HOPS complex with Syntaxin 17 mediates autophagosome clearance in Drosophila. Mol Biol Cell 2014;25:1338–1354
16. Pols MS, van Meel E, Oorschot V, et al. hVps41 and VAMP7 function in direct TGN to late endosome transport of lysosomal membrane proteins. Nat Commun 2013;4:1361
17. Keller MP, Choi Y, Wang P, et al. A gene expression network model of type 2 diabetes links cell cycle regulation in islets with diabetes susceptibility. Genome Res 2008;18:706–716
18. Accelerating Medicines Partnership. Type 2 Diabetes Knowledge Portal: VPS41, 2019. Accessed 11 November 2020. Available from https://t2d.hugeamp.org/region.html?chr=7&end=39021994&phenotype=T2D&start=38712563
19. Asensio CS, Sirkis DW, Maas JW Jr., et al. Self-assembly of VPS41 promotes sorting required for biogenesis of the regulated secretory pathway. Dev Cell 2013;27:425–437
20. van der Welle REN, Jobling R, Burns C, et al. VPS41 recessive mutation causes ataxia and dystonia with retinal dystrophy and mental retardation by inhibiting HOPS function and mTORC1 signaling. bioRxiv. 20 December 2019 [preprint]. DOI: 10.1101/2019.12.18.867333
21. Cong L, Ran FA, Cox D, et al. Multiplex genome engineering using CRISPR/Cas systems. Science 2013;339:819–823
22. Witwicka H, Hwang SY, Reyes-Gutierrez P, et al. Studies of OC-STAMP in osteoclast fusion: a New knockout mouse model, rescue of cell fusion, and transmembrane topology. PLoS One 2015;10:e0128275
23. Hummer BH, Maslar D, Soltero-Gutierrez M, de Leeuw NF, Asensio CS. Differential sorting behavior for soluble and transmembrane cargoes at the *trans*-Golgi network in endocrine cells. Mol Biol Cell 2020;31:157–166
24. Slot JW, Geuze HJ. Cryosectioning and immunolabeling. Nat Protoc 2007;2:2480–2491
25. Kuliawat R, Klumperman J, Ludwig T, Arvan P. Differential sorting of lysosomal enzymes out of the regulated secretory pathway in pancreatic beta-cells. J Cell Biol 1997;137:595–608
26. Aoyama M, Sun-Wada GH, Yamamoto A, Yamamoto M, Hamada H, Wada Y. Spatial restriction of bone morphogenetic protein signaling in mouse gastrula through the mVam2-dependent endocytic pathway. Dev Cell 2012;22:1163–1175
27. Boncompain G, Divoux S, Gareil N, et al. Synchronization of secretory protein traffic in populations of cells. Nat Methods 2012;9:493–498
28. Thorens B, Tarussio D, Maestro MA, Rovira M, Heikkilä E, Ferrer J. Ins1(Cre) knock-in mice for beta cell-specific gene recombination. Diabetologia 2015;58:558–565
29. Brereton MF, Iberl M, Shimomura K, et al. Reversible changes in pancreatic islet structure and function produced by elevated blood glucose. Nat Commun 2014;5:4639
30. Marsh BJ, Soden C, Alarcón C, et al. Regulated autophagy controls hormone content in secretory-deficient pancreatic endocrine beta-cells. Mol Endocrinol 2007;21:2255–2269
31. Halban PA. Structural domains and molecular lifestyles of insulin and its precursors in the pancreatic beta cell. Diabetologia 1991;34:767–778
32. Orci L, Ravazzola M, Amherdt M, et al. Insulin, not C-peptide (proinsulin), is present in crinophagic bodies of the pancreatic B-cell. J Cell Biol 1984;98:222–228
33. Pasquier A, Vivot K, Erbs E, et al. Lysosomal degradation of newly formed insulin granules contributes to β cell failure in diabetes. Nat Commun 2019;10:3312
34. Riahi Y, Wikstrom JD, Bachar-Wikstrom E, et al. Autophagy is a major regulator of beta cell insulin homeostasis. Diabetologia 2016;59:1480–1491
35. Yamaguchi H, Arakawa S, Kanaseki T, et al. Golgi membrane-associated degradation pathway in yeast and mammals. EMBO J 2016;35:1991–2007
36. Csizmadia T, Lőrincz P, Hegedűs K, Széplaki S, Lőw P, Juhász G. Molecular mechanisms of developmentally programmed crinophagy in *Drosophila*. J Cell Biol 2018;217:361–374
37. Asensio CS, Sirkis DW, Edwards RH. RNAi screen identifies a role for adaptor protein AP-3 in sorting to the regulated secretory pathway. J Cell Biol 2010;191:1173–1187
38. Cao M, Mao Z, Kam C, et al. PICK1 and ICA69 control insulin granule trafficking and their deficiencies lead to impaired glucose tolerance. PLoS Biol 2013;11:e1001541
39. Holst B, Madsen KL, Jansen AM, et al. PICK1 deficiency impairs secretory vesicle biogenesis and leads to growth retardation and decreased glucose tolerance. PLoS Biol 2013;11:e1001542
40. Paquin N, Murata Y, Froehlich A, et al. The conserved VPS-50 protein functions in dense-core vesicle maturation and acidification and controls animal behavior. Curr Biol 2016;26:862–871
41. Pinheiro PS, Jansen AM, de Wit H, et al. The BAR domain protein PICK1 controls vesicle number and size in adrenal chromaffin cells. J Neurosci 2014;34:10688–10700
42. Sasidharan N, Sumakovic M, Hannemann M, et al. RAB-5 and RAB-10 cooperate to regulate neuropeptide release in Caenorhabditis elegans. Proc Natl Acad Sci U S A 2012;109:18944–18949
43. Sirkis DW, Edwards RH, Asensio CS. Widespread dysregulation of peptide hormone release in mice lacking adaptor protein AP-3. PLoS Genet 2013;9:e1003812
44. Zhang X, Jiang S, Mitok KA, Li L, Attie AD, Martin TFJ. BAIAP3, a C2 domain-containing Munc13 protein, controls the fate of dense-core vesicles in neuroendocrine cells. J Cell Biol 2017;216:2151–2166
45. Topalidou I, Cattin-Ortolá J, Hummer B, Asensio CS, Ailion M. EIPR1 controls dense-core vesicle cargo retention and EARP complex localization in insulin-secreting cells. Mol Biol Cell 2020;31:59–79
46. Topalidou I, Cattin-Ortolá J, Pappas AL, et al. The EARP complex and its interactor EIPR-1 are required for cargo sorting to dense-core vesicles. PLoS Genet 2016;12:e1006074
47. Ni Q, Gu Y, Xie Y, et al. Raptor regulates functional maturation of murine beta cells. Nat Commun 2017;8:15755
48. Gilleron J, Gerdes JM, Zeigerer A. Metabolic regulation through the endosomal system. Traffic 2019;20:552–570